

Abundances and Kinematics of Field Stars II: Kinematics and Abundance Relationships

Jon P. Fulbright¹
Dominion Astrophysical Observatory, Herzberg Institute of Astrophysics, National Research Council,
5071 West Saanich Road, Victoria, BC V8X-4M6, Canada. Email: Jon.Fulbright@nrc.ca

Received December 14, 2000; accepted September 28, 2001

arXiv:astro-ph/0110164v1 8 Oct 2001

ABSTRACT

As an investigation of the origin of “ α -poor” halo stars, we analyze kinematic and abundance data for 73 intermediate metallicity stars ($-1 > [\text{Fe}/\text{H}] \geq -2$) selected from Paper I of this series. We find evidence for a connection between the kinematics and the enhancement of certain element-to-iron ($[\text{X}/\text{Fe}]$) ratios in these stars. Statistically significant correlations were found between $[\text{X}/\text{Fe}]$ and galactic rest-frame velocities (v_{RF}) for Na, Mg, Al, Si, Ca and Ni, with marginally significant correlations existing for Ti and Y as well. We also find that the $[\text{X}/\text{Fe}]$ ratios for these elements all correlate with a similar level of significance with $[\text{Na}/\text{Fe}]$. Finally, we compare the abundances of these halo stars against those of stars in nearby dSph galaxies. We find significant differences between the abundance ratios in the dSph stars and halo stars of similar metallicity. From this result, it is unlikely that the halo stars in the solar neighborhood, including even the “ α -poor” stars, were once members of disrupted dSph galaxies similar to those studied to date.

1. Introduction

Traditionally, the chemical enrichment history of the Galaxy is described to follow the general scenario given by Tinsley (1979). In this scenario, the metal-poor halo stars formed from the ejecta of short-lived Type II supernovae. These events eject material rich in the so-called “ α -elements” (here taken as O, Mg, Si, Ca, and Ti). Observed halo stars, which presumably formed from this gas, preserved this pattern by showing $[\alpha/\text{Fe}]$ ratios of $\sim +0.3$. About 1 Gyr after the initial burst, Type Ia supernovae began exploding, ejecting Fe-group rich material. This explains the observed drop of the $[\alpha/\text{Fe}]$ ratio from the halo value at $[\text{Fe}/\text{H}] \sim -1$ to solar at $[\text{Fe}/\text{H}] \sim 0$ (Edvardsson *et al.* 1993; McWilliam 1997).

More recently studies have found halo stars that do not follow this pattern of α -element enhancement. Carney *et al.* (1997), King 1997, and Hanson *et al.* (1998, hereafter H98) all found stars with $[\alpha/\text{Fe}]$ ratios lower than what is normally expected for halo stars. The globular clusters Ruprecht 106 and Palomar 12 (Brown *et al.* (1997)) also show $[\alpha/\text{Fe}]$ ratios that are relatively low (for their metallicity) compared to the majority of the halo. The most exceptional case is BD +80 245, which shows near-solar $[\alpha/\text{Fe}]$ ratios at $[\text{Fe}/\text{H}] \sim -2$ (Carney *et al.* 1997). These ratios suggest a different chemical enrichment history for these stars than for the rest of the halo.

Kinematics may help determine the origin of these stars. Carney *et al.* (1997) noted that the known metal-poor halo stars with unusual abundances all have high apogalactic radii, while H98 found that more of the stars with lower $[\text{Na}/\text{Fe}]$ ratios move on retrograde orbits. It should be possible, using the large, self-consistent sample of Fulbright (2000, hereafter F00) to test whether or not stars on extreme orbits demonstrate unusual element abundance ratios.

The F00 data set includes the LTE analysis of 15 elements based on high resolution, high signal-to-noise echelle spectra of 168 stars. These stars were selected primarily by metallicity from lists of known metal-poor stars or by their potential as being subdwarfs from their location on a Hipparcos-based color-magnitude diagram. All of the observed stars are members of the Hipparcos catalog. In addition to these 168 stars, an additional 11 stars with equivalent width measurements from Stephens (1999, hereafter S99), were reanalyzed following the same procedure. The analysis procedure of F00 followed a self-consistent methodology aimed at producing the most accurate abundance measurements possible.

One suggestion for the origin of the α -poor stars is that these stars may have been accreted since the formation of the rest of the stellar halo. Smecker-Hane & Wyse (1992) and Gilmore & Wyse

(1998) have suggested that dwarf galaxies or proto-galactic fragments may have chemical enrichment histories with lower α -element enhancements. While it not possible to determine absolutely the origin of individual field stars, the abundances of stars within potential future accretion targets (e.g., Milky Way satellite dSph galaxies) should follow patterns similar to what Smecker-Hane & Wyse or Gilmore & Wyse suggest. The recent abundance analysis of Shetrone *et al.* (2001) of stars within 3 nearby dSph galaxies allows such comparisons to be made in one potential source of accreted stars.

This paper will be organized as follows: In Section 2 of this paper, we will calculate kinematic parameters for the F00 stars and select a sample for further study. The data will then be used to demonstrate that there exist correlations between abundance ratios and kinematics and that there are correlations between the element enhancements of certain light elements (Section 3). Finally, in Section 4 we will show that true analogues to the α -poor halo stars do not exist in the Milky Way satellite dSph galaxies studied to date.

2. Data Used in the Analysis

2.1. Abundance Data

The abundance ratios from F00 are presented in Figures 1–3. Also plotted are stars from several recent abundance surveys. As can be seen, there is significant overlap for metal-rich stars between the F00 data and the data of Edvardsson *et al.* (1993) and Clemintini *et al.* (1999). In the extremely metal-poor regime ($[\text{Fe}/\text{H}] \lesssim -2$), the Ryan *et al.* 1991 and the McWilliam *et al.* (1995) data provide more stars than F00, but the intermediate metallicity range ($-2 < [\text{Fe}/\text{H}] < -1$) is nearly exclusively covered by the F00 data.

Figure 4 presents comparisons of a few of the abundance ratios measured by both F00 and the other surveys. There is an overall good agreement between the F00 results and previous surveys, except for a ~ 0.1 dex offset in $[\text{Si}/\text{Fe}]$. The origin of this offset is unclear—the atomic data used for Si by the different surveys all agree well, and the sensitivity of $[\text{Si}/\text{Fe}]$ to systematic errors in the stellar parameters (see Table 8 of F00) is smaller than the values measured for other $[\text{X}/\text{Fe}]$ ratios that do not show a similar offset.

2.2. Kinematic Data

As stated in F00, one of the selection criteria for this survey is inclusion in the Hipparcos Catalog (ESA 1997). All of the proper motions and positions used in this survey come from the catalog. With the exception of several giants whose Hipparcos parallaxes are uncertain, all of the adopted distances are derived from Hipparcos parallaxes. We adopt the H98 or Anthony-Twarog & Twarog (1994) distances (giving preference to H98) for those giants with Hipparcos $\delta(\pi)/\pi > 0.2$.

The adopted radial velocities (see Table 1) come from several sources, most often the Carney *et al.* (1994) survey and the Hipparcos Input Catalog (ESA 1992). Other radial velocities were adopted from the literature. For the remaining stars we measured radial velocities from the spectra themselves. No calibrations to radial velocity standards were made, but for the 73 stars in common with Carney *et al.* (1994), the mean difference in the observed heliocentric radial velocity (F00 – CLLA) is $+0.3 \pm 3.9$ km s^{-1} (sdm), and for the 38 stars with radial velocities adopted from the Hipparcos Input Catalog the mean difference (F00 – HIC) is $+1.9 \pm 4.4$ km s^{-1} .

Given the above input parameters, the UVW velocities for the stars were calculated using a set of programs kindly provided by R. Hanson (private communication). The UVW velocities are defined such that positive U values denote motion away from the Galactic Center, positive V values are in the direction of the solar motion, and positive W values are parallel to the direction of the North Galactic Pole. The UVW components were transformed to the local standard of rest (LSR) using the solar motion $(U_{\odot}, V_{\odot}, W_{\odot})_{LSR} = (-9, 12, 7 \text{ km s}^{-1})$ (Mihalas and Binney, p. 400). For purposes of this paper, the rotational velocity of the LSR with respect to the Galaxy was set to 220 km/s^{-1} and the galactocentric distance was set to 8.5 kpc. Also given in Table 1 are the galactic rest frame velocities, $v_{RF} (= \sqrt{U_{LSR}^2 + (V_{LSR} + 220)^2 + W_{LSR}^2})$, orbital velocities in the direction of the Sun’s orbit, $v_{ROT} (= V_{LSR} + 220 \text{ km s}^{-1})$ and specific angular momentum values, $h (= \sqrt{v_{ROT}^2 + W_{LSR}^2})$.

Orbital parameters for each star (maximum and minimum galactocentric radii, R_{max} and R_{min} , maximum absolute distance from the galactic plane, $|Z_{max}|$, and orbital eccentricity, e) were calculated using an integrator kindly provided by D. Lin (1999, private communication). The integrator uses a three component potential describing the halo, disk, and bulge and is described in more detail by Johnston (1998). Each star was followed for 5 Gyr or at least 8 orbits. Table 1 lists the resulting kinematic and orbital parameter values. For completeness, the stars from S99 are listed with kinematic parameters from the Carney *et al.* (1994) survey, but the orbital parameters were recalculated using the same galactic potential model as the F00 stars.

2.3. Selection of Stars for Further Study

An important kinematic parameter is the rest-frame velocity of the star with respect to the center of mass of the Galaxy (v_{RF}). Carney (1999) notes that the known α -poor stars show high galactic rest-frame velocities. If we wish to test whether this is true, we need to ensure that our sample does not exclude these important stars. In Figure 5 we plot $[\text{Fe}/\text{H}]$ against v_{RF} and find that the F00 data set does not include a large number of very metal-poor ($[\text{Fe}/\text{H}] < -2$), high-velocity stars. This is most likely a selection effect, as the high-velocity star study of Carney *et al.* (1988) found that out of a sample of 24 stars with $v_{RF} > 375 \text{ km/s}^{-1}$, 13 have $-1 > [\text{Fe}/\text{H}] \geq -2$ and 10 showed $[\text{Fe}/\text{H}] < -2$. Most of the very metal-poor, high-velocity stars included in Carney *et al.* (1988) were too faint to be included in the F00 survey, and only the availability of the S99 data made it possible to include a reasonable number of high-velocity stars.

Also included in Figure 5 are stars from Edvardsson *et al.* (1993) sample of disk stars. As can be seen, for the metal-rich stars ($[\text{Fe}/\text{H}] > -1$) the F00 and Edvardsson *et al.* (1993) samples share the same regions. Similar comparisons of the other kinematic and orbital parameters between the two samples in this metallicity range lead us to believe that the stars with $[\text{Fe}/\text{H}] > -1$ in the F00 sample are almost all members of the disk population.

Therefore, to ensure a less biased comparison of stars, we will generally confine our discussion of the relationship between kinematics and abundances to the 73 stars with $-1 < [\text{Fe}/\text{H}] < -2$, as demarked by the dotted lines in Figure 5. For simplicity, we will refer to this set of stars as the “selected sample” for the remainder of the paper. Note that the selected sample does not include the well-know $\alpha - poor$ star BD +80245.

3. Abundances as a Function of Kinematic Properties

3.1. [X/Fe] vs. v_{RF}

In this section, we will test whether stars showing extreme orbital parameters show different abundance parameters than stars on more normal orbits. A useful kinematic parameter for these comparisons is v_{RF} , as defined above. This parameter is directly related to the star’s kinetic energy with respect to the Galaxy. The value of v_{RF} is determined solely from observational data and, unlike R_{max} , is independent of the model is used to describe the galactic gravitational potential.

As a quantitative way to describe any trends with v_{RF} , we fit least-squares lines to the distributions of [X/Fe] vs. v_{RF} for the selected sample. In Figures 6 and 7 we plot the fits to the eight element ratios that are somewhat significant. For the fits involving Na, Mg, Al, Si, Ca, and Ni, the value of the correlation coefficients are such that there is a less than 0.05% chance that the correlations are random. For the fits involving Ti and Y, the probability is a few percent. These significance levels were confirmed by a non-parametric Spearman rank-order analysis, which compares only the rank order of the two variables and is independent of the form of the correlation. Fits to the other element ratios (including [Fe/H]) did not show any significant correlations. For simplicity, we will refer to the [X/Fe] ratios for Na, Mg, Al, Si, Ca and Ni as the “varying” ratios.

To further explore the potential relationship between [X/Fe] and v_{RF} , we divide the selected sample into three v_{RF} groups. The properties of these three groups are given in Table 2 and the mean values of [X/Fe] are plotted in Figure 8. The three groups have a similar mean T_{eff} and [Fe/H] values, but the highest velocity group has a higher mean value of $\log g$. This is due to the inclusion of the S99 stars to help fill out the highest velocity group. Even among metal-poor stars high velocity stars are rare. The S99 stars were specifically selected for their kinematics from the Carney *et al.* (1994) survey, which primarily included dwarf stars. The F00 survey selection was mainly based on metallicity which allowed more evolved stars into the survey.

Figure 8 demonstrates that the highest velocity stars have a different distribution of light elements. The mean values of both [Na/Fe] and [Mg/Fe] are ~ 0.2 dex lower for the high velocity group, while the mean values of [Al/Fe], [Si/Fe], [Ca/Fe], [Y/Fe] and [Ba/Fe] are slightly lower as well. The error bars in Figure 8 represent the standard deviation of the mean within each bin for that element ratio. They do not include the estimated random errors in the observations of the ratios (~ 0.1 dex, as discussed in F00).

Besides the relatively low light element abundance ratios, it is possible that the highest velocity stars also show slightly lower ratios of the s-process elements Y, Zr, and Ba. The mean [Ba/Eu] ratio does show a change between the velocity groups, but this measurement is limited by the number of Eu measurements. A lower s-process fraction in these stars would suggest that chemical evolution history of these stars contains less recycling of the ejecta from AGB stars, the suspected site of the main s-process. The size of the s-process deficiency is small and may not be significant, so an enlarged sample of high-quality s-process element ratios should help clarify this picture.

3.2. Element-Element Correlations

The trends in Figures 6–8 suggest that the light element ratios may be correlated with each other. If this is the case, then [Na/Fe], which shows the largest range star-to-star variations in [X/Fe], could be used as a surrogate for describing the overall enhancements of these element ratios. Indeed, H98 and

Snedden (1998) present evidence that there is a correlation between $[\text{Na}/\text{Fe}]$ and $[\text{Mg}/\text{Fe}]$ in halo giant stars. Here we attempt to expand this to other element ratios.

For the selected sample, we made linear least-squares fits to the $[\text{X}/\text{Fe}]$ vs. $[\text{Na}/\text{Fe}]$ distributions. As a comparison, fits were also made to the $[\text{X}/\text{Fe}]$ vs. $[\text{Fe}/\text{H}]$ distributions as well. We find strongly significant relationships between $[\text{Na}/\text{Fe}]$ and the other varying ratios. Correlations significant to the few percent level were found for the fits with $[\text{Ti}/\text{Fe}]$ and $[\text{Y}/\text{Fe}]$. For the fits using $[\text{Fe}/\text{H}]$ as the independent variable, only $[\text{Cr}/\text{Fe}]$ shows a strongly significant correlation. The above significance levels were confirmed through the use of Spearman rank-order tests.

Another confirmation comes from the relative size of the standard deviations of the $[\text{X}/\text{Fe}]$ values around the least squares fits ($\sigma_{[\text{X}/\text{Fe}]}$). For the five ratios that strongly correlate with $[\text{Na}/\text{Fe}]$, the values of $\sigma_{[\text{X}/\text{Fe}]}$ found for the fit to $[\text{Na}/\text{Fe}]$ are $\sim 30\%$ smaller than those found for the fit to $[\text{Fe}/\text{H}]$. For the remaining ratios, the $\sigma_{[\text{X}/\text{Fe}]}$ values were comparable between the fits to the different independent variables.

In Figure 9 we plot the $[\text{X}/\text{Fe}]$ vs. $[\text{Na}/\text{Fe}]$ distributions for the four α -elements studied in F00. All four ratios show trends with $[\text{Na}/\text{Fe}]$, but as a further test, we calculated the value of $[\alpha/\text{Fe}]$ (the mean of the $[\text{X}/\text{Fe}]$ ratios for Mg, Si, Ca and Ti) for the 65 stars in the selected sample having abundance measurements for all four elements. The plot of $[\alpha/\text{Fe}]$ vs. $[\text{Na}/\text{Fe}]$ is presented in the top panel of Figure 10. The quality of the fit and the statistical significance is better than the fits to the individual ratios themselves. Also plotted in Figure 10 are the $[\text{X}/\text{Fe}]$ vs. $[\text{Na}/\text{Fe}]$ distributions and fits for Al, Ni and Y.

Random and systematic errors in the stellar parameters (T_{eff} , $\log g$, etc.) could possibly lead to the correlations seen here. Table 8 of F00 gives the effects of specific changes in the stellar parameters on the final abundance ratios. For most of the varying elements, the sign of the changes all match, meaning that the errors are correlated. However, the magnitude of the changes are too small with respect to the variations seen in the elements. For example, a change of 150 K in T_{eff} , a 0.2 dex change in $\log g$, or a 0.3 km s^{-1} change in the microturbulent velocity results in a change of ~ 0.05 dex or less in the resulting abundances. The change in parameter values needed to explain the range of $[\text{X}/\text{Fe}]$ values seen is unreasonable. Also, the lines used in F00 were specifically chosen to ensure that the individual lines of a given element have consistent results as compared to the other lines of that element over a wide range of stellar parameters. Because of the care taken to form the line list it is unlikely, short of problems with the basic assumptions of the LTE, plane-parallel analysis, that the results seen here are artifacts of line selection or the abundance analysis.

3.3. Abundances and Orbital Parameters

Instead of using v_{RF} as the kinematic parameter, Carney *et al.* (1997) and Carney (1999) noted potential trends between R_{max} or h and abundances. Using $[\text{Na}/\text{Fe}]$ as a surrogate for the other varying element ratios, we can test these trends with the F00 data set. Plots of $[\text{Na}/\text{Fe}]$ against orbital parameters are shown in Figures 10(a)–(c). The fraction of “Na-poor” stars (those with $[\text{Na}/\text{Fe}] < -0.36$) increases for $R_{\text{max}} > 20$ kpc (9 of 22 stars) and $|Z_{\text{max}}| > 5$ kpc (5 of 10 stars). From these counts, about a half of extreme halo stars should show lower element ratios. Conversely, 55% (6 of 11) of stars with $[\text{Na}/\text{Fe}] < -0.36$ have $R_{\text{max}} > 40$ kpc, while only 6% of the remaining sample has values of R_{max} this high. Ten of the 11 Na-poor stars have $v_{\text{RF}} > 300$ km s^{-1} , while only 11 of the 113 other stars have this high a value of v_{RF} .

Carney (1999) suggested that the previously observed alpha-poor stars also had high “specific angular momentum” (h) values. For any star, the maximum value of $|h|$ is v_{RF} . For the 11 stars with $[\text{Na}/\text{Fe}] < -0.36$, the mean value of $|h|/v_{\text{RF}}$ is 0.78 ± 0.07 (sdom). If the one star (G197-30) with an $|h|/v_{\text{RF}}$ value of 0.17 is eliminated, the mean value increases to 0.84 ± 0.04 . This compares to a mean value of 0.66 ± 0.04 for the other 61 stars in the selected sample with $[\text{Na}/\text{Fe}]$ abundances.

4. Accretion Origin of the α -poor Stars?

So far we have shown that the highest velocity stars in the solar neighborhood show a different pattern of abundance ratios than the lower velocity stars. This suggests that these stars did not form in the same manner than the rest of the halo. One theory for the origin of the low- α halo stars is that they were accreted from the cannibalization of other stellar systems. If the stellar halo of the Milky Way was made up of disrupted and accreted proto-galactic fragments, as suggested by Cote *et al.* (2000), then studies of stars within present-day dwarf galaxies (assuming they are products of similar fragments) may help explain the abundance patterns seen in the halo. Shetrone *et al.* (2001) analyzed high-resolution spectra of 17 giants stars in the Draco, Ursa Minor and Sextans dwarf spheroidal (dSph) galaxies. Their methodology is similar to the LTE analysis technique employed by F00, although the spectra were of lower S/N (~ 15 – 35) than F00.

In Figure 12, we plot the mean $[\text{X}/\text{Fe}]$ values for the 10 Shetrone *et al.* (2001) dSph stars with $-1 > [\text{Fe}/\text{H}] \geq -2$ along with the 3 kinematic groups of the selected sample stars. For several elements the mean values of the $[\text{X}/\text{Fe}]$ ratios differ between the dSph stars and the halo stars. It is also clear that the dSph abundance pattern does not match what is seen in α -poor stars. For example, the most extreme α -poor star known, BD +80245 (= HIP 40068) shows $[\text{Ba}/\text{Fe}]$ and $[\text{Eu}/\text{Fe}]$ ratios ~ 1.5 dex below halo stars of similar metallicity (see Figure 3). This would place it off the bottom of Figure 12, while the mean dSph values for these two ratios is higher than the mean halo value.

Since the F00 survey did not find any stars with abundance pattern similar to the dSph stars, it is unlikely that a large fraction of the field halo stars in the solar neighborhood, including the α -poor stars, are former members of dSph galaxies of the kind studied by Shetrone *et al.* (2001).

Despite this, continued high-resolution work on individual stars in other galaxies may find an extragalactic origin for the α -poor stars. For example, Hill *et al.* (2000) present O and Al abundances derived from high-quality high-resolution spectra of 10 giants in globular clusters associated with the LMC. For the stars that do not show signs of deep mixing (enhanced $[\text{Al}/\text{Fe}]$ and depressed $[\text{O}/\text{Fe}]$), the general trend of the metal-poor stars is to have low values of $[\text{O}/\text{Fe}]$ and $[\text{Al}/\text{Fe}]$ compared to unmixed Galactic globular cluster giants. The analysis of a full range of elements in the stars is necessary before further comparisons can be made. However, one exciting prospect is that the LMC cluster system shows a range of ages (see Elson & Fall 1988 and Geisler *et al.* 1997), so it may be possible to explore the effects of time of formation on abundance ratios.

5. Discussion and Future Work

In this paper, we have presented observational evidence that shows that the $[\text{X}/\text{Fe}]$ ratios for certain elements decline in concert for higher values of v_{RF} . Here we discuss some possible scenarios that may produce the pattern of elements found in the high velocity stars.

The production of Na and Mg by Type II supernova is dominated by massive progenitor stars with M

$> 30M_{\odot}$ (see Figure 6 of McWilliam 1997 and Woosley & Weaver 1995), while the lower mass progenitors create relatively more of the heavier α - and Fe-group elements. A possible explanation for the decline of the light elements without a similar decline in the heavier elements is to decrease the relative fraction of very massive stars in the chemical enrichment history of the α -poor stars. The connection of IMF slope to location in the Galactic potential (assuming that the stars with higher v_{RF} formed at greater distances from the Galactic center) is unclear.

Another possibility is incomplete mixing. Using a single Salpeter IMF, Argast *et al.* (2000) ran simulations of the chemical enrichment history of the early Galaxy and included provisions for incomplete mixing. They found that incomplete mixing can explain the presence of star-to-star variations for the light element ratios for the moderately metal-poor stars, but if the mixing in the halo was less complete at high v_{RF} , one would expect to see high-velocity stars with relatively high values of $[\text{Na}/\text{Fe}]$, $[\text{Mg}/\text{Fe}]$, etc. as well.

Alternatively, the lower $[\text{X}/\text{Fe}]$ ratios for some elements may be due to extra Fe-rich material being added to the gas that formed the stars that are now at high v_{RF} . Type Ia supernovae could be the source of the Fe-group enrichment. There are, however, a few observational details that do not agree with this theory:

First, other element ratios like $[\text{Ca}/\text{Fe}]$ and $[\text{Ti}/\text{Fe}]$ do not show the same level of decrease with v_{RF} . Nucleosynthesis models of Type Ia SN do suggest these events create a reasonable amount of Ca and Ti (Nomoto *et al.* 1997), but it is unclear whether or not these kind of events can keep the mean $[\text{Ti}/\text{Fe}]$ value approximately constant. Second, these same models predict an overproduction of Ni with respect to Fe by Type Ia SN. If anything, the mean $[\text{Ni}/\text{Fe}]$ ratio in the high velocity stars is lower than for the rest of the halo (see Figure 8).

Some of these issues could possibly be resolved by careful analysis of additional elements. Oxygen, for example, should be formed mainly by the very massive Type II supernovae. That means the $[\text{O}/\text{Fe}]$ ratio should track $[\text{Na}/\text{Fe}]$ and $[\text{Mg}/\text{Fe}]$. By a similar argument, $[\text{S}/\text{Fe}]$ should follow $[\text{Si}/\text{Fe}]$. There may also be clues in the other Fe-group and heavier elements on the relative contributions of Type Ia and II supernovae. We are in the process of analyzing many of these elements in the F00 spectra.

Another natural next step is to observe more high velocity stars, such as those listed in Carney *et al.* (1988) or elsewhere in the literature. The 11-star survey of S99 found seven Na-poor stars using kinematic selection criteria. These stars are rare, and therefore faint, require time on 8- to 10-m class telescopes to build up a sizable sample. However, it is also important to continue observing lower velocity stars in order to search for Na-poor stars in their midst. It is paramount to resolve the potential NLTE effects in the abundance analysis through either consistent sample selection or, preferably, accurate stellar atmosphere modelling. Finally, it cannot be stressed enough that any such new survey needs to follow some sort of self-consistent analysis procedure for all the stars, even if it is not the same one followed in F00. Any procedure should also include the analysis of a wide sample of stars for comparisons, as for this type of work accurate relative abundances are more important than the absolute overall scaling.

6. Summary of Results

From the analysis of the self-consistent abundance analysis of F00, combined with Hipparcos-based kinematics, we have found:

1. The general trends of the element-to-iron ratios with respect to $[\text{Fe}/\text{H}]$ are similar to those seen

by previous studies.

2. For intermediate-metallicity ($-2 < [Fe/H] < -1$) stars from F00, the $[X/Fe]$ ratios for Na, Mg, Al, Si, Ca and Ni, as well as possibly Ti and Y show a decrease in the value of $[X/Fe]$ with increasing v_{RF} .

3. For the metal-poor stars the values of $[X/Fe]$ for the above elements are correlated. The correlation between $[\alpha/Fe]$ and $[Na/Fe]$ is show a higher significance than between any of the individual $[X/Fe]$ ratios and $[Na/Fe]$.

4. When compared to the field halo sample, the dSph giant sample of Shetrone *et al.* (2001) shows a different pattern of abundance ratios than the field halo sample, including the high v_{RF} stars. It is unlikely that the α -poor stars in the solar neighborhood originated the dSph galaxies similar to those studied by Shetrone *et al.* (2001).

The papers of this series make up the PhD thesis of JPF at the University of California at Santa Cruz. JPF wishes to thank the members of his committee (R. Kraft, R. Peterson, M. Bolte and P. Gahathakurta) for their efforts and advice. JPF also wishes to thank B. Hanson for his assistance with the Hipparcos catalog and the codes for calculating UVW components for the sample stars, D. Lin for the codes used in calculating the orbits of the sample stars and J. Johnson and V. Weafer for reviewing drafts of this paper. Special thanks should got to the anonymous referee for their useful comments. This research was supported by NSF contract AST 96-18351 to R. P. Kraft and by the National Research Council of Canada.

REFERENCES

- Anthony-Twarog, B. J. & Twarog, B. A. 1994, *AJ*, 107, 1994
- Argast, D., Samland, M., Gerhard, O. E. & Thielemann, F.-K. 2000, *A&A*, 356, 873
- Bartkevicius, A., Sperauskas, J., Rastorguev, A. S. & Tokovinin, A. A. 1992, *BaltA*, 1, 47
- Beers, T. C. & Sommer-Larsen, J. 1995, *ApJS*, 96, 175
- Beers, T. C., Chiba, M., Yoshii, Y., Hanson, R. B., Fuchs, B. & Rossi, S. 2000, *AJ*, 119, 2866
- Bond, H. E. 1980, *ApJS*, 44, 517
- Brown, J. A., Wallerstein, G., & Zucker, D. 1997, *AJ*, 114, 180
- Carney, B. W., Latham, D. W. & Laird, J. B. 1988, *AJ*, 98, 560
- Carney, B. W., Latham, D. W., Laird, J. B. & Aguilar, L. A. 1994, *AJ*, 107, 2240 (CLLA)
- Carney, B. W., Laird, J. B., Latham, D. W. & Aguilar, L. A. 1996, *AJ*, 112, 668
- Carney, B. W., Wright, J. S., Sneden, C., Laird, J. B., Aguilar, L. A. & Latham, D. W. 1997, *AJ*, 114, 363
- Carney, B. W. 1999, in *ASP Conf. Ser. 165, The Galactic Halo*, ed. B. K. Gibson *et al.* (San Francisco: ASP), 230
- Chiba, M. & Yoshii, Y. 1998, *AJ*, 115, 168.
- Clemintini, G., Gratton, R. G., Carretta, E. & Sneden, C. 1999, *MNRAS*, 302, 22.
- Cote, P., Marzke, R. O., West, M. J. & Minniti, D. 2000, *ApJ*, 533, 869
- Edvardsson, B., Andersen, J., Gustafsson, B., Lambert, D. L., Nissen, P. E. & Tomkin, J. 1993, *A&A*, 275, 101
- Elson, R. A. W. & Fall, S. M. 1988, *AJ*, 96, 1383
- ESA 1992, *The Hipparcos Input Catalogue*, European Space Agency Publication SP-1136
- ESA 1997, *The Hipparcos and Tycho Catalogues* (ESA SP-1200) (Noordwijk: ESA)
- Fulbright, J. P. 2000, *AJ*, 120, 1841 (F00)
- Geisler, D., Bica, E., Dottori, H., Claria, J. J., Paitti, A. E. & Santos, J. F. C, Jr. 1997, *AJ*, 114, 1920
- Gilmore, G. & Wyse, R. F. G. 1998, *AJ*, 116, 748
- Hanson, R. B., Sneden, C., Kraft, R. P. & Fulbright, J. P. 1998, *AJ*, 116, 1286 (H98)
- Hill, V., Francois, P., Spite, M., Primas, F. & Spite, F. 2000, *A&A*, 364, 19

- Johnston, K. V. 1998, ApJ, 495, 297
- King, J. R. 1997, AJ, 113, 2302
- McWilliam, A., Preston, G. W., Sneden, C., & Searle, L. 1995, AJ, 109, 2757
- McWilliam, A. 1997, ARA&A, 35, 503
- Mihalas, D. & Binney, J. 1981, Galactic Astronomy (2nd ed.; San Francisco: Freeman)
- Nomoto, K., Iwamoto, K., Nakasato, N., Thielemann, F.-K., Brachwitz, F., Tsujimoto, T., Kubo, Y. & Kishimoto, N. 1997, Nucl. Phys. A, 621, 467
- Norris, J. 1986, ApJS, 61, 667
- Ryan, S. G., Norris, J. E. & Bessell, M. S. 1991, AJ, 102, 303
- Sangage, A. & Fouts, G. 1987, AJ, 93, 74
- Shetrone, M. D., Cote, P. & Sargent, W. L. W. 2001, ApJ, 548, 592
- Smecker-Hane, T. A. & Wyse, R. F. G. 1992, AJ, 104, 144
- Sneden, C. 1998, in IAU Symp. 187, in press
- Stephens, A. 1999, AJ, 117, 1771 (S99)
- Stetson, P. B. 1983, AJ, 88, 1349
- Tinsley, B. M. 1979, ApJ, 229, 1046
- Woosley, S. E. and Weaver, T. A. 1995, ApJS, 101, 181

Fig. 1.— Fulbright.fig1.ps

The distribution of $[X/Fe]$ vs. $[Fe/H]$ for Na, Mg, Al and Si for the F00 and other recent abundance surveys. The estimated measurement errors for the F00 data are shown in the upper right. The F00 star with low $[X/Fe]$ at $[Fe/H] = -2.05$ for several panels in Figures 1–3 is the star BD +80245 (= HIP 40068), first studied by Carney *et al.* (1997).

Fig. 2.— Fulbright.fig2.ps

Same as Figure 1, but for Ca, Ti, V, Cr and Ni.

Fig. 3.— Fulbright.fig3.ps

Same as Figure 1, but for Y, Zr, Ba and Eu. As mentioned in F00, the $[Eu/Fe]$ measurement for BD +80245 is an upper limit.

Fig. 4.— Fulbright.fig4.ps

Comparison of the measured abundance ratios for stars in common between F00 and the other abundance surveys included in Figures 1–3. As discussed in the text, the $[Si/Fe]$ ratio shows a ~ 0.1 dex offset between the F00 and other surveys.

Fig. 5.— Fulbright.fig5.ps

The distribution of $[Fe/H]$ vs. v_{RF} for the F00 data. There is a lack of very metal-poor ($[Fe/H] < -2$) high velocity stars, although such stars are known to exist. For the metal-rich ($[Fe/H] > -1$) stars, the F00 and Edvardsson *et al.* (1993) disk stars cover the same region, suggesting that the more metal-rich F00 stars are members of the disk population. The dotted lines denote the intermediate metallicity “selected sample.”

Fig. 6.— Fulbright.fig6.ps

Plots of the distribution of $[X/Fe]$ vs. v_{RF} for Na, Mg, Al and Si for the selected sample. All four of these distributions show statistically significant correlations with respect to v_{RF} . The solid line is the least-squares fit to the data, while the dotted line is the reverse least-squares fit. The estimated measurement uncertainty for the abundance ratios is shown in the lower left.

Fig. 7.— Fulbright.fig7.ps

Same as Figure 6, but for Ca, Ti, Ni and Y. The correlations for Ti and Y are not as significant as the other six elements. The other elements studied in F00 (V, Cr, Zr, Ba and Eu) do not show any statistically significant correlations with v_{RF} .

Fig. 8.— Fulbright.fig8.ps

Figure 8. Plots of the mean value of $[X/Fe]$ for the selected sample broken into three v_{RF} groups. The highest velocity group has significantly lower mean values for several elements. Note that the number of measurements for any given ratio may be smaller than the number of stars in that group. This is especially a problem for Al, which helps explain the large *sdom* error bars for that ratio.

Fig. 9.— Fulbright.fig9.ps

Plots of the correlation between the $[X/Fe]$ ratios for the four α -elements measured in F00 and $[Na/Fe]$. The symbols are the same as in Figure 8, and the error bars denote the estimated measurement uncertainty for the ratios. As in Figures 6 and 7, the solid line marks the least-squares fit to the data,

while the dotted line is the reverse fit. The displacement of the high velocity stars to lower $[X/Fe]$ values is clear in these plots.

Fig. 10.— Fulbright.fig10.ps

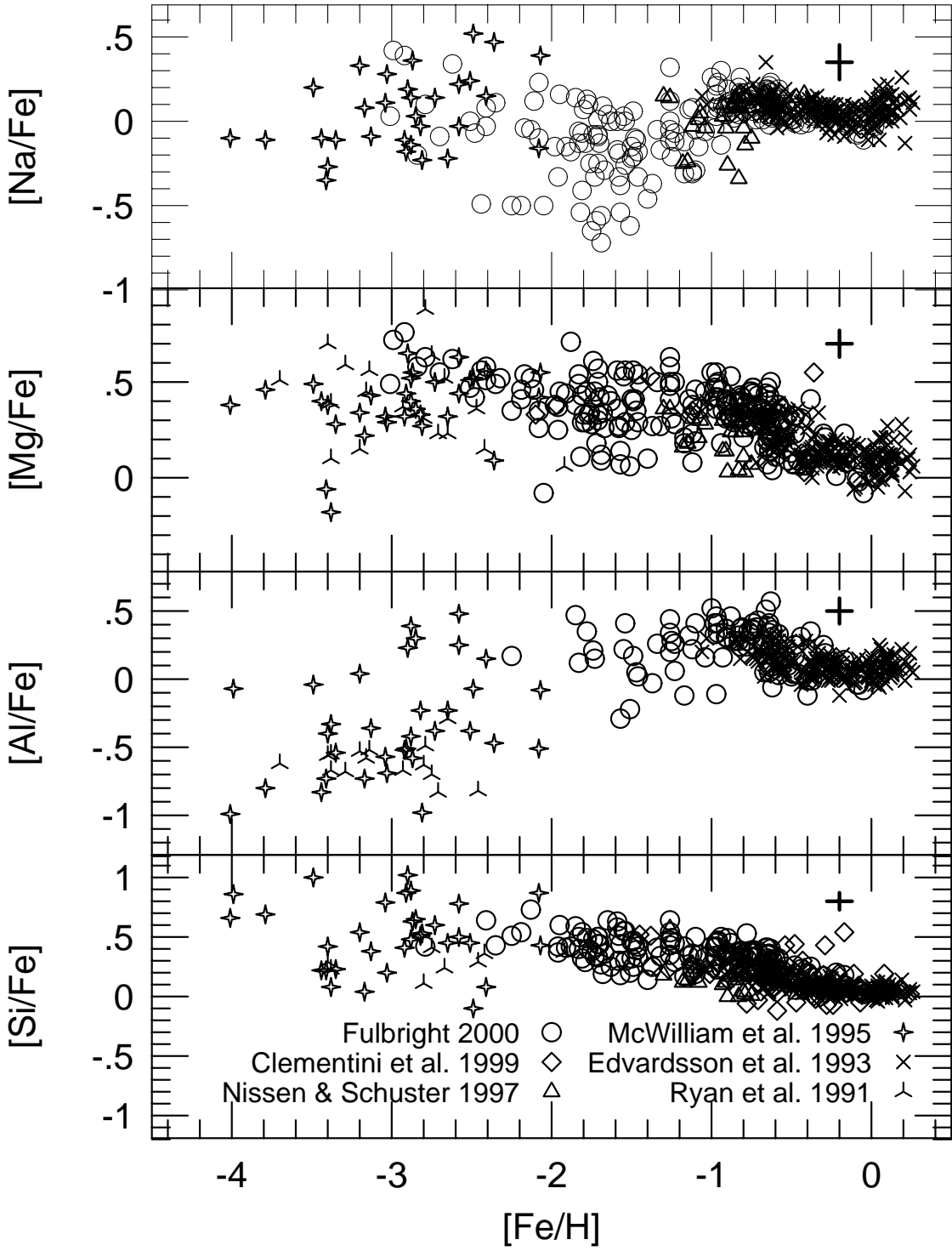
Same as Figure 9, but for the mean α -element abundance (for only the 65 stars with measurements of all four elements), Al, Ni, and Y. The statistical significance of the $[\alpha/Fe]$ vs. $[Na/Fe]$ correlation is greater than any of the four individual α -elements with $[Na/Fe]$.

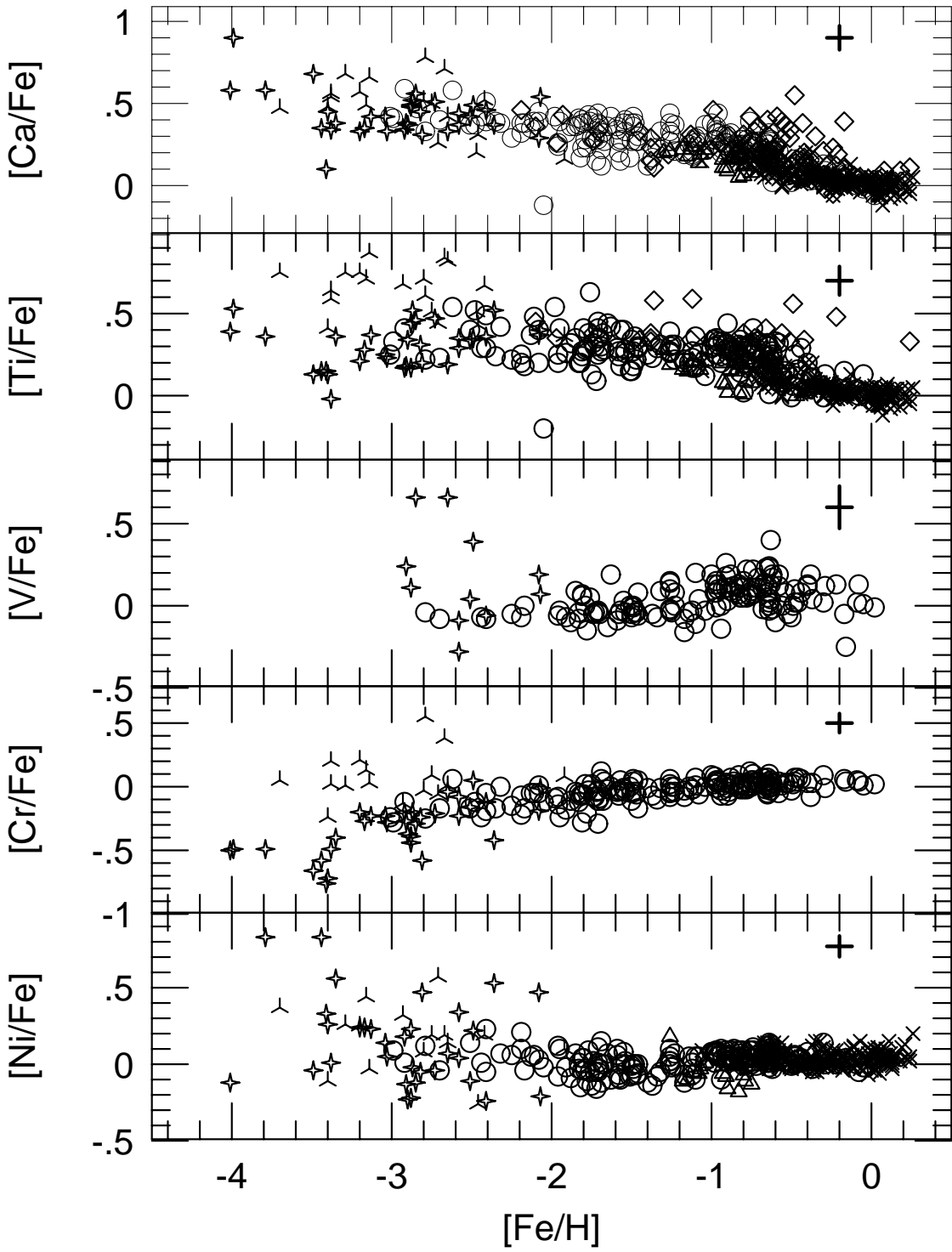
Fig. 11.— Fulbright.fig11.ps

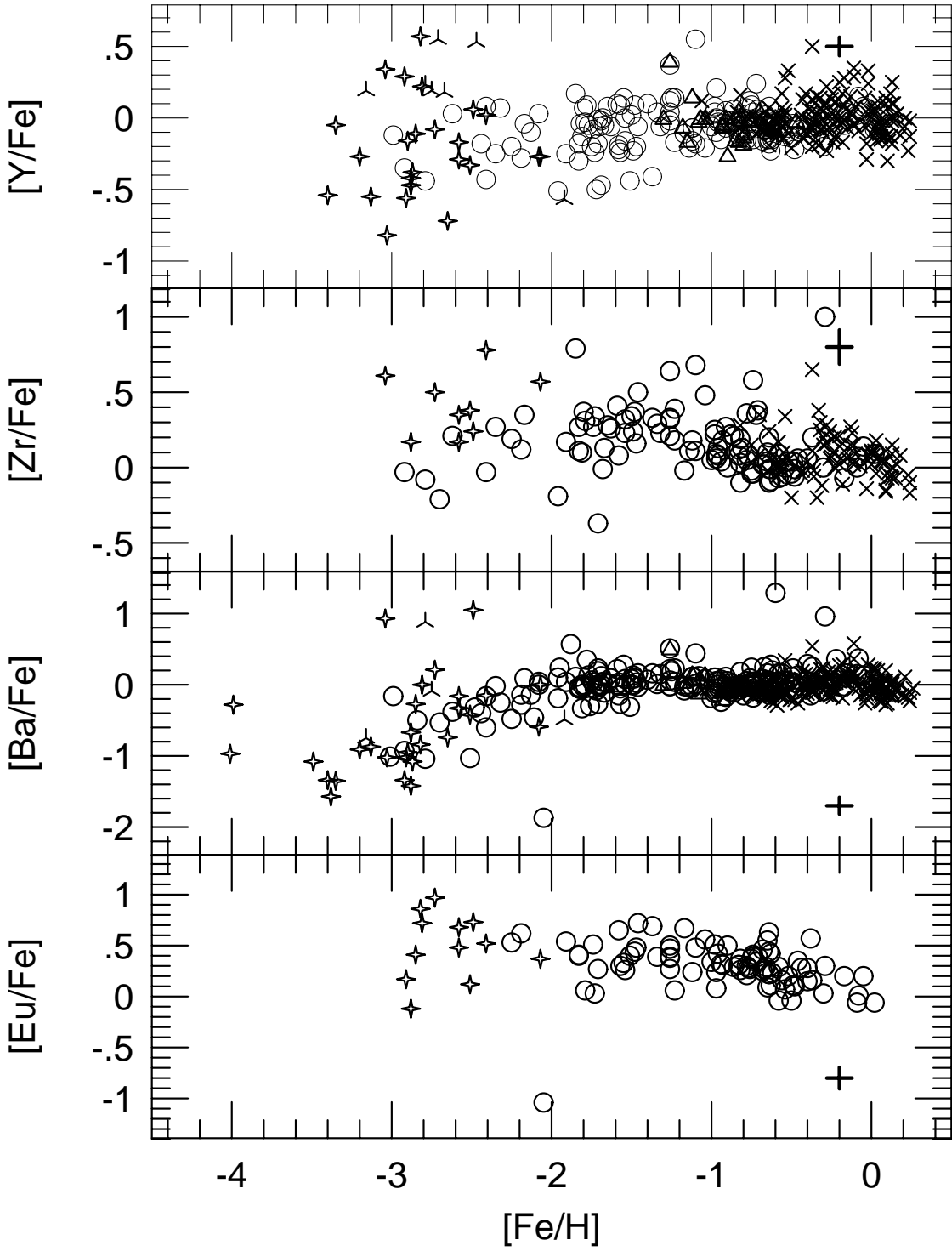
The value of $[Na/Fe]$ as a function of R_{max} and $|Z_{max}|$ for the selected sample. The symbols are the same as in Figure 8, and the dotted line denotes the mean $[Na/Fe]$ ratio of the highest v_{RF} group ($[Na/Fe] = -0.36$). Approximately half of the stars with $R_{max} > 20$ kpc or $|Z_{max}| > 5$ kpc show $[Na/Fe]$ ratios lower than nearly all of the lower v_{RF} halo stars.

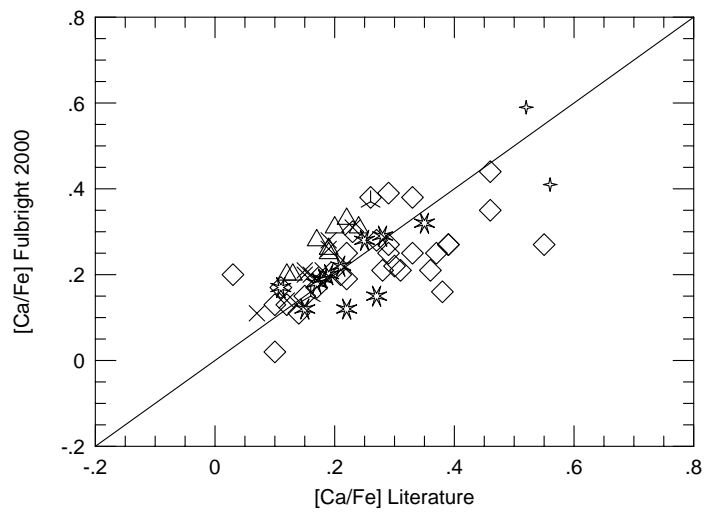
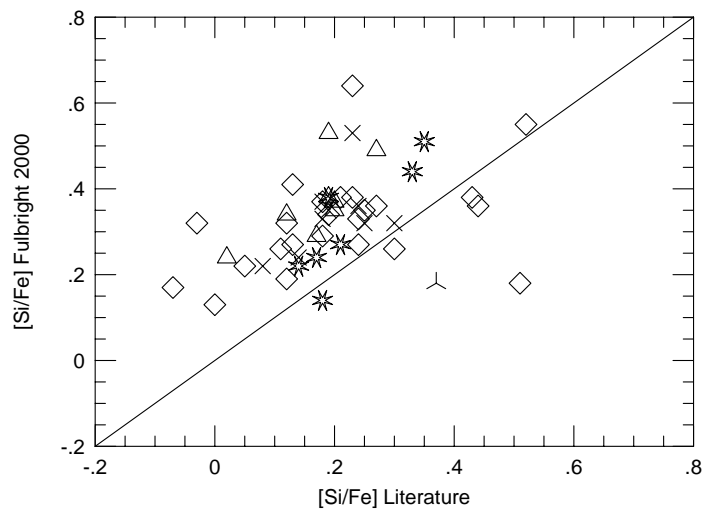
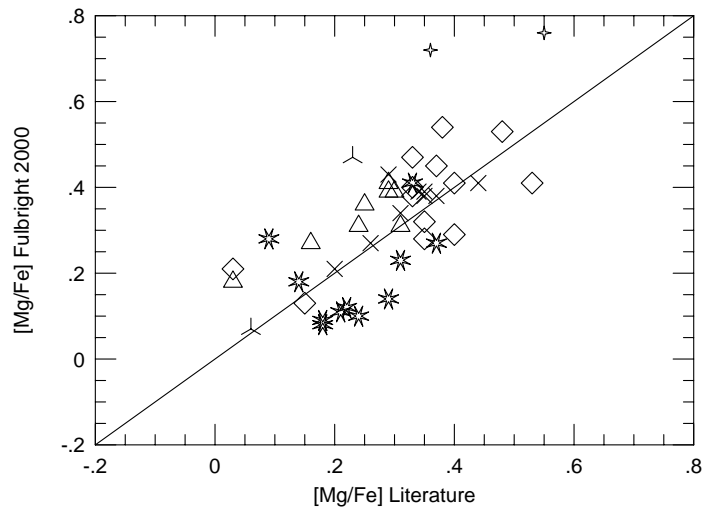
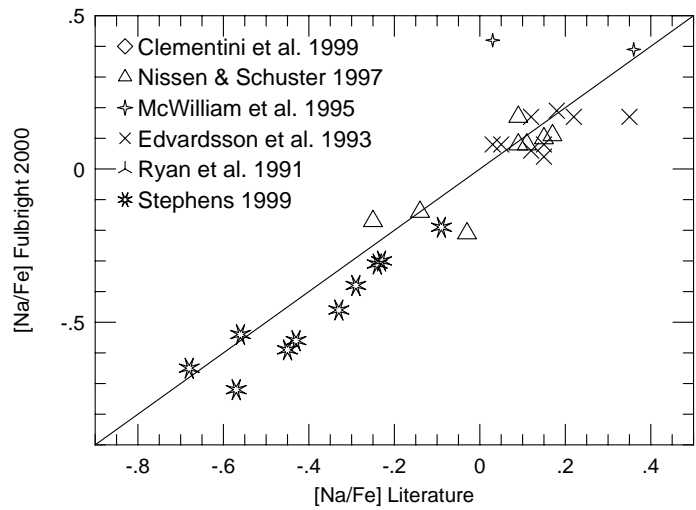
Fig. 12.— Fulbright.fig12.ps

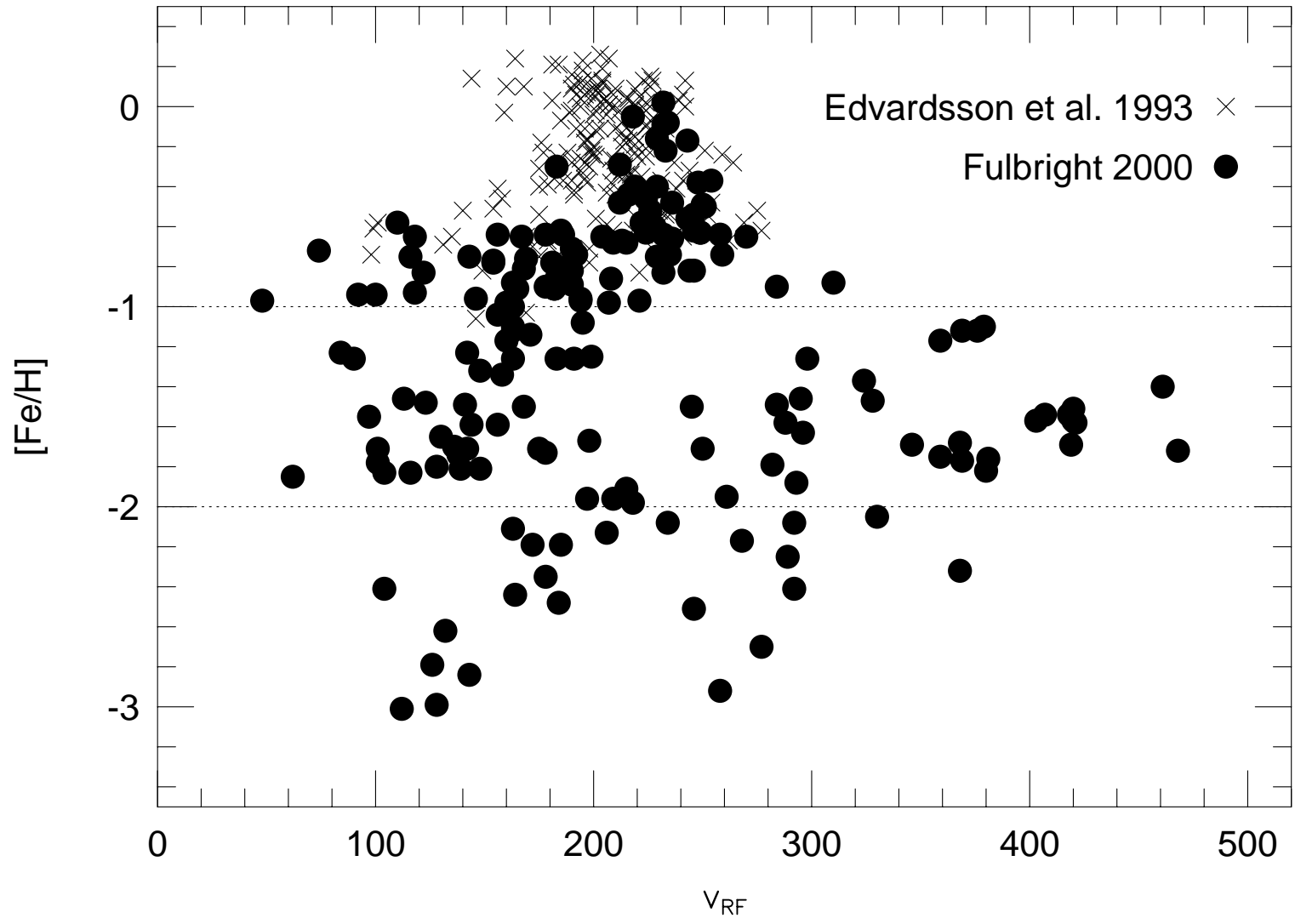
Same as Figure 8, but with the mean $[X/Fe]$ ratios for the intermediate metallicity dSph stars from Shetrone *et al.* (2001) plotted as well. While the dSph stars show similar mean values to the high velocity stars for some elements, the large differences seen in the mean ratios for Ca, Ti, Cr, Y, Ba and Eu strongly suggest that the high velocity stars were not accreted from disrupted dSph galaxies like the ones observed by Shetrone *et al.* (2001).

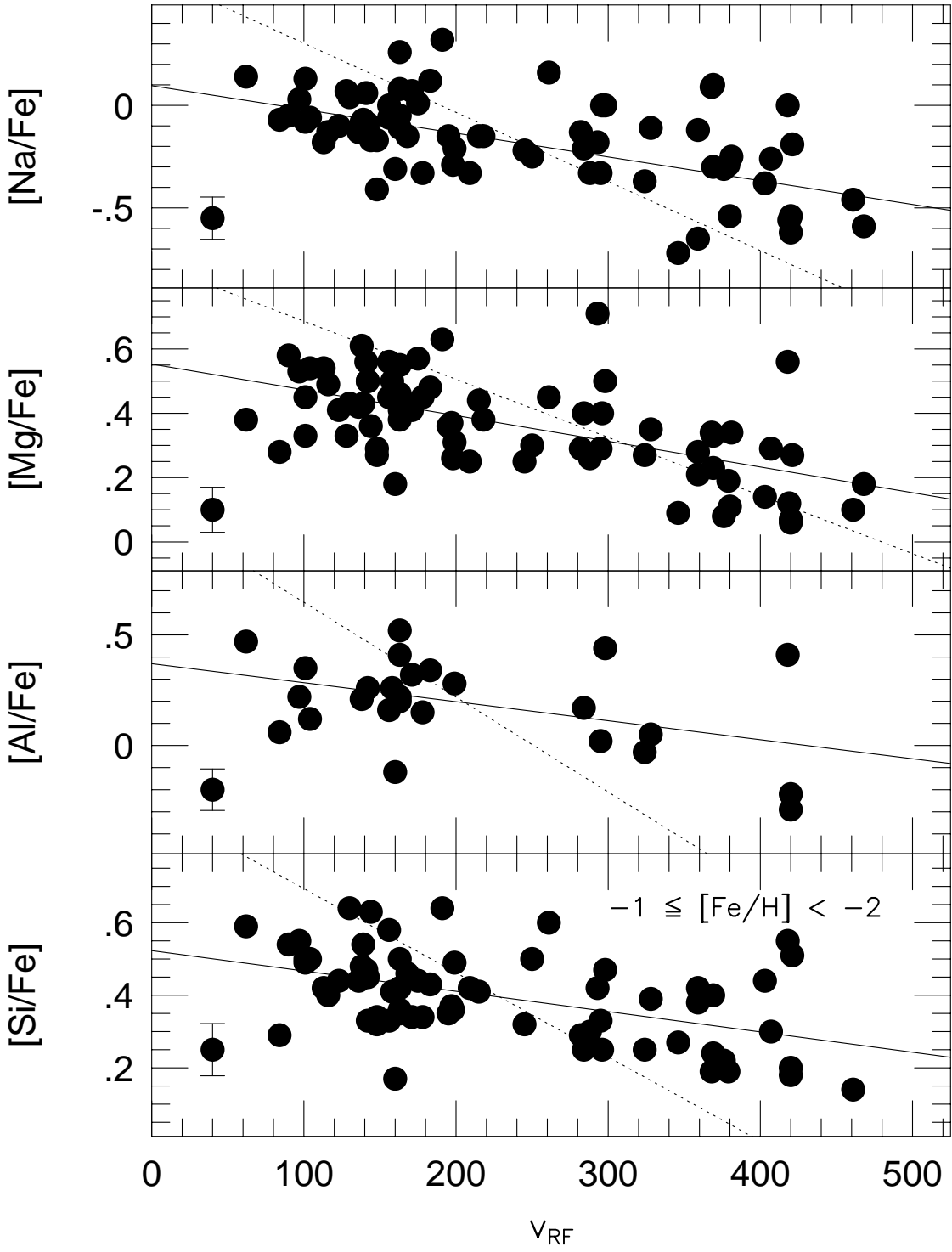


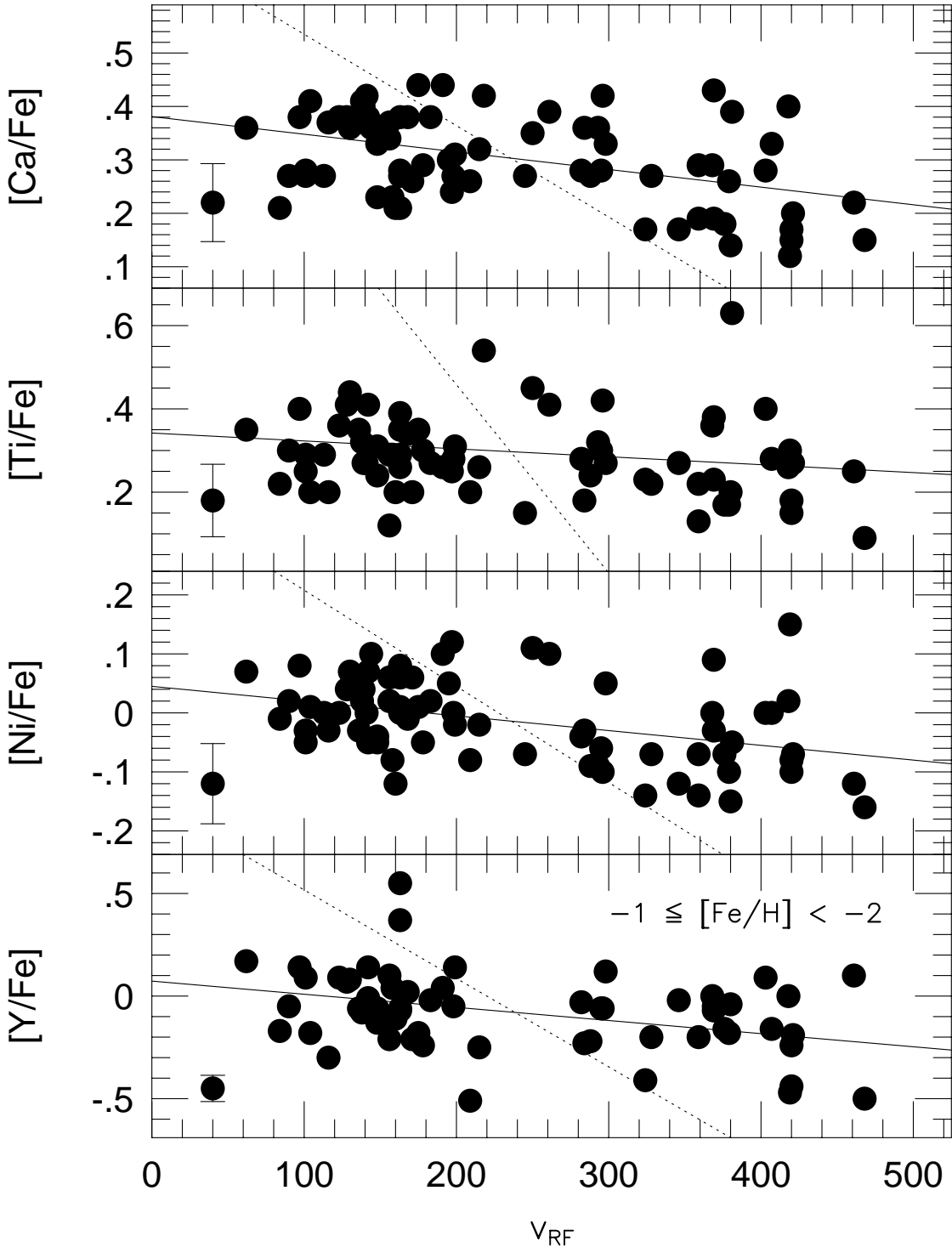


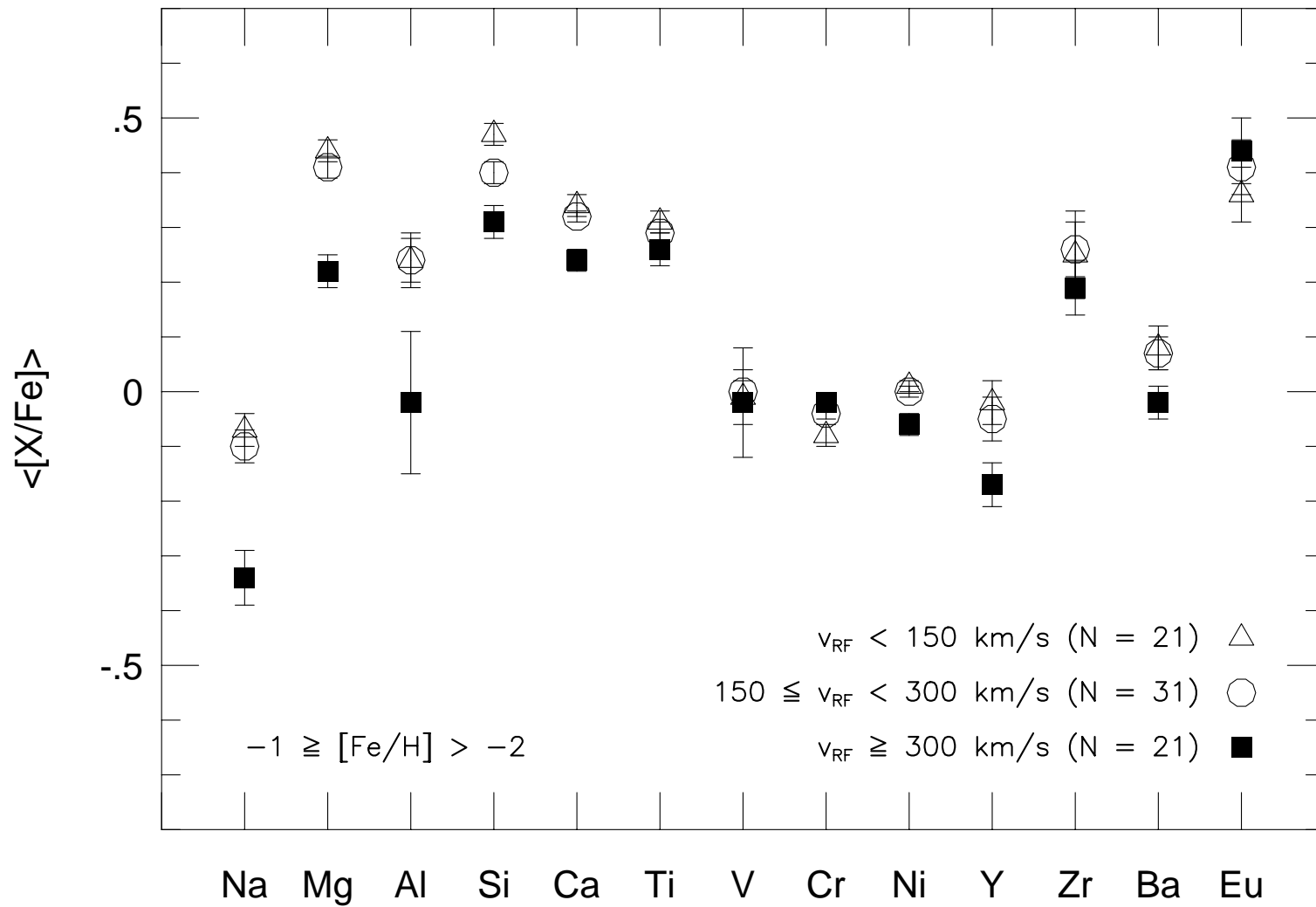


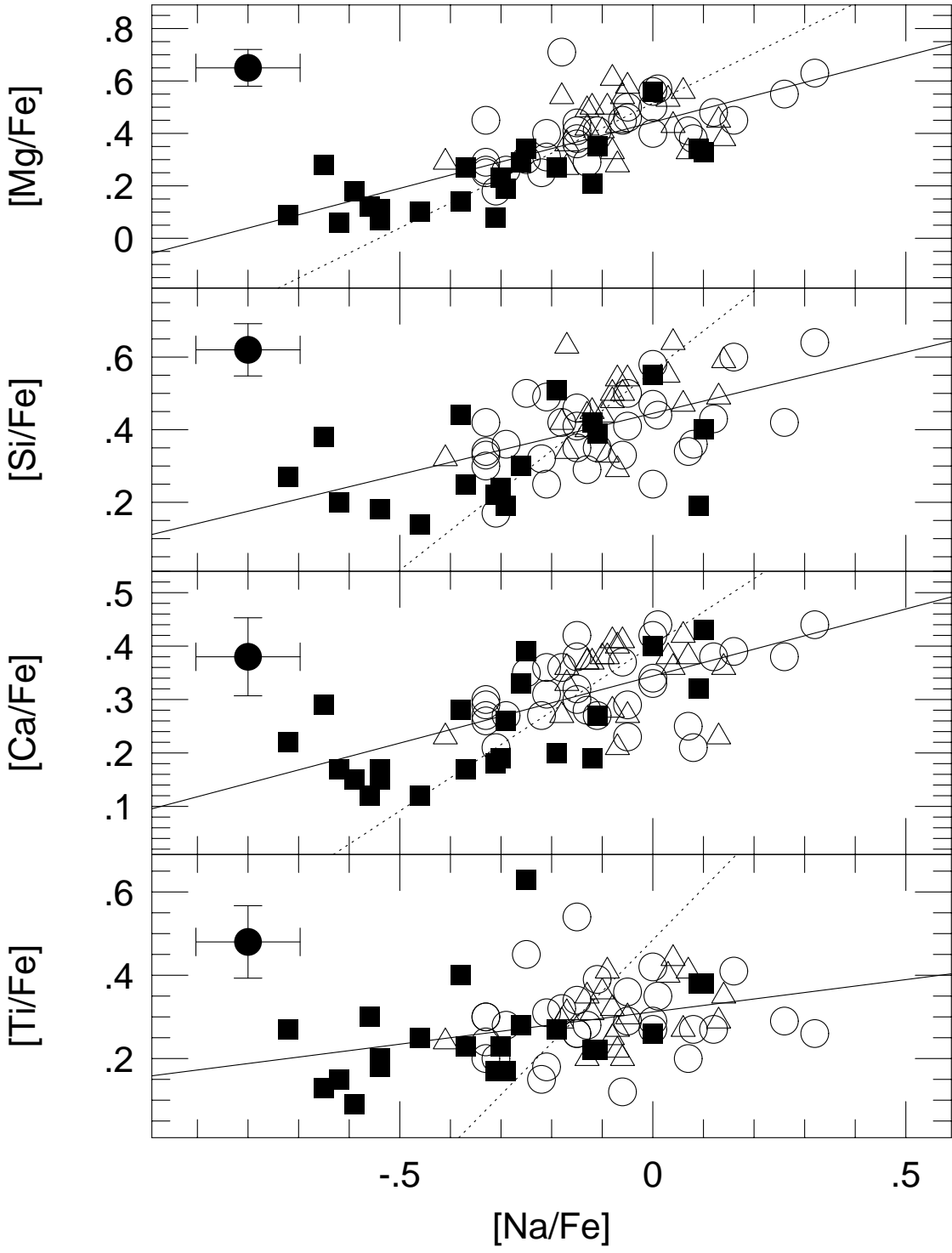


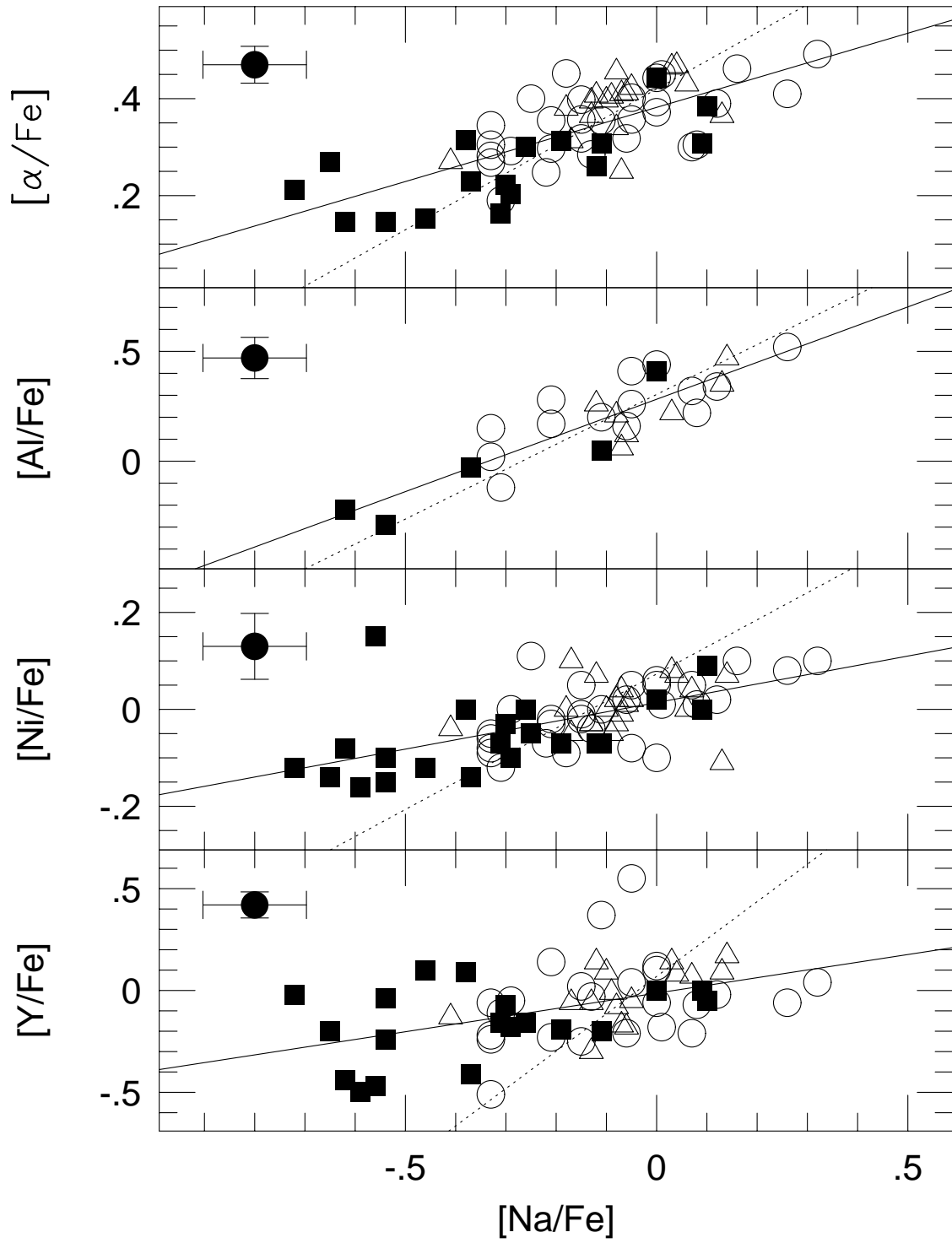


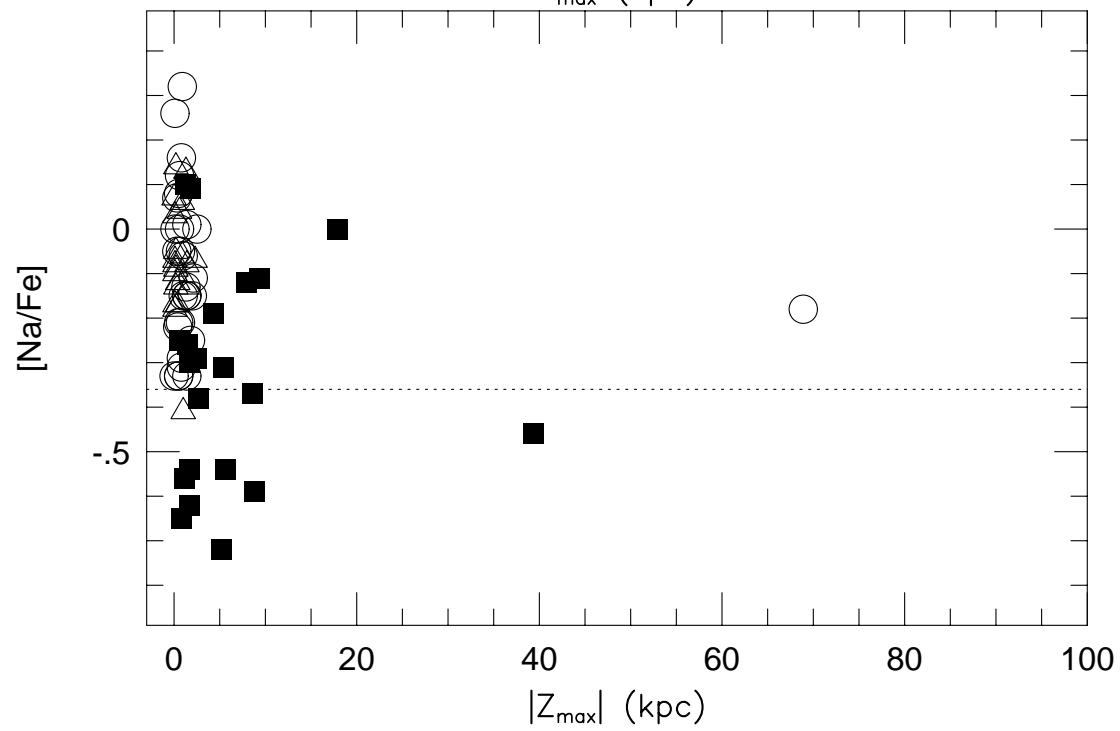
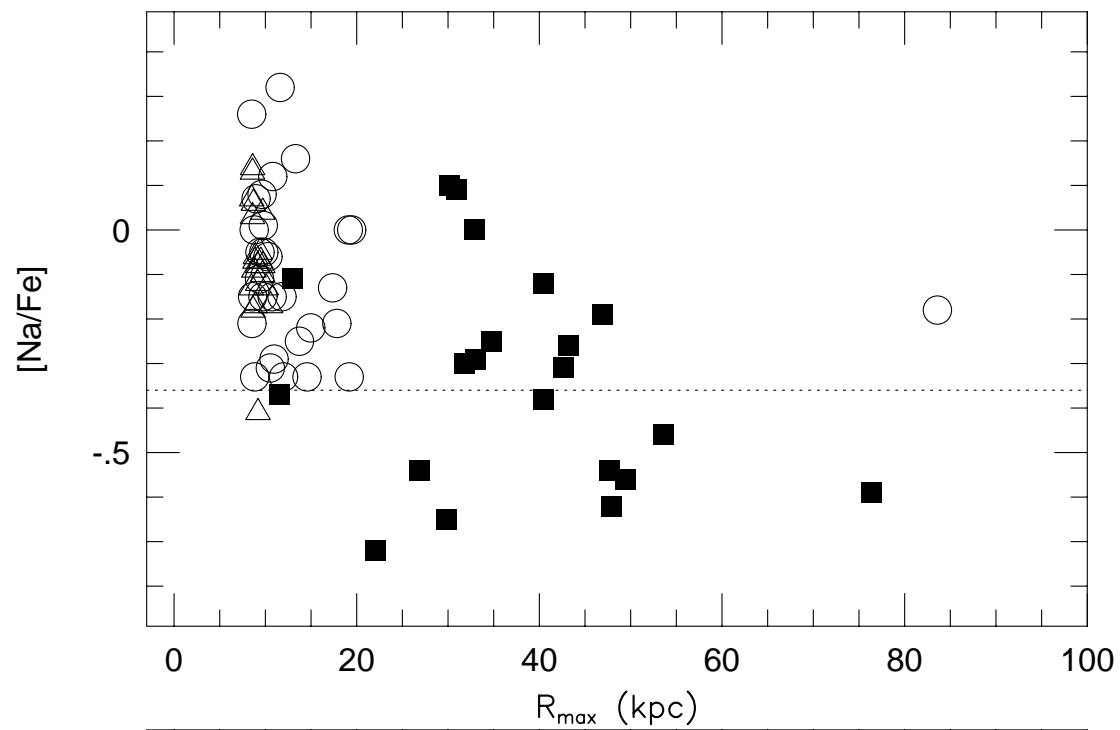












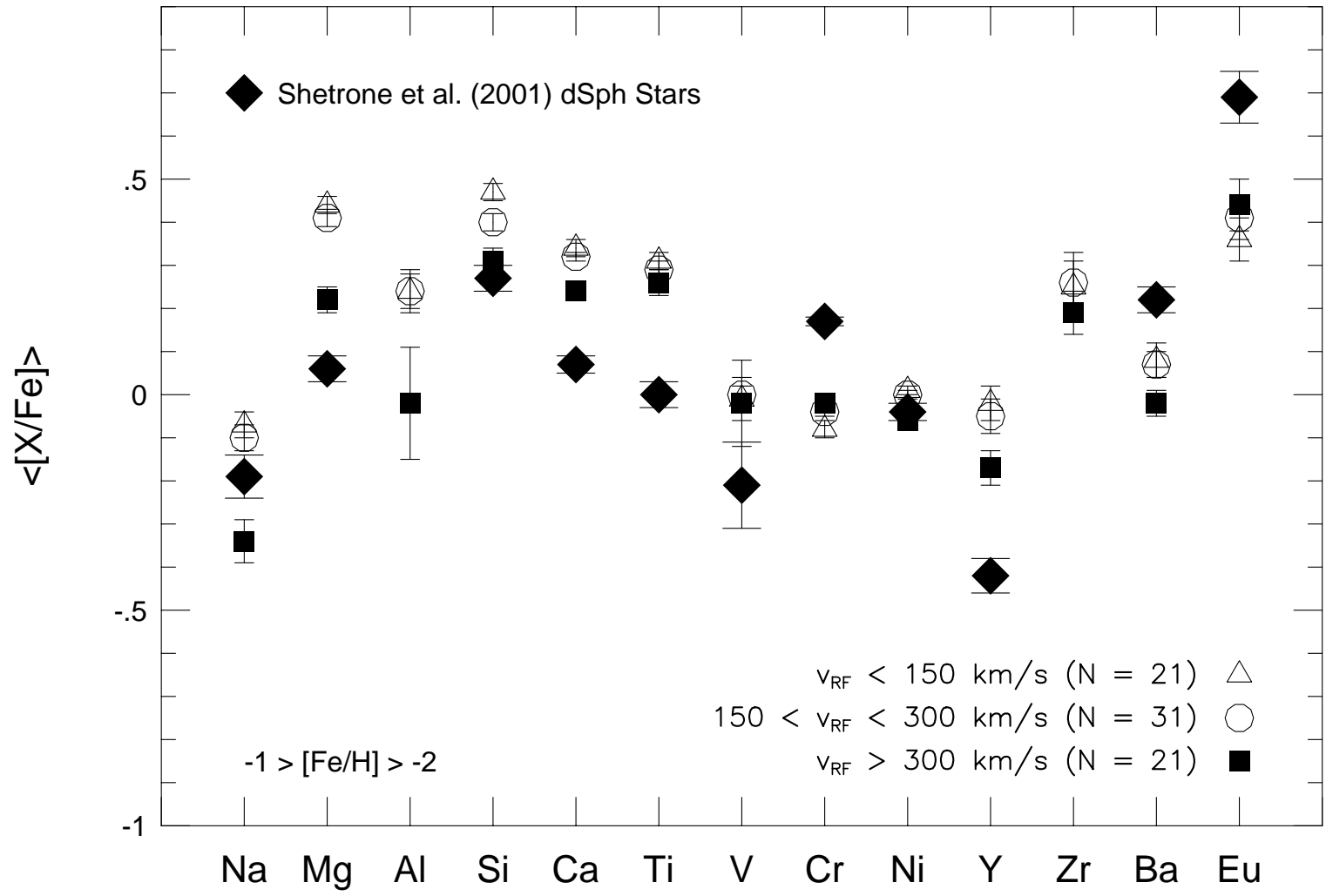


TABLE 1. Kinematic and Orbital Data

HIP ^a	RV km/s	Ref ^b	U_{LSR} km/s	V_{LSR} km/s	W_{LSR} km/s	v_{RF} km/s	v_{ROT} km/s	h km/s	R_{min} kpc	R_{max} kpc	e	$ Z_{max} $ kpc
SUN	-9	12	7	232	232	232	8.4	8.9	0.03	0.1
171	-36	1	-1	-59	-23	163	161	163	4.7	8.5	0.29	0.2
2413	-378	4	-161	-345	-46	209	-125	-133	2.7	12.0	0.64	0.5
3026	-49	2	-144	-223	-34	148	-3	34	0.0	10.4	0.99	0.4
3086	-28	2	156	-42	55	243	178	186	4.3	12.8	0.49	0.7
3554	-67	1	177	-55	86	258	165	187	3.9	14.1	0.57	2.2
5336	-24	2	96	-41	-41	207	179	183	4.3	10.2	0.35	0.4
5445	-321	1	118	-468	89	288	-248	-263	6.9	14.6	0.36	1.4
5458	-245	1	-131	-192	81	156	28	85	0.5	10.3	0.91	1.0
6710	-110	1	-14	-300	-64	104	-80	-103	1.8	8.9	0.66	1.0
7217	-53	2	-102	-8	-9	236	212	212	6.0	11.3	0.30	0.1
10140	27	2	52	-63	-41	171	157	162	4.4	9.0	0.34	0.4
10449	28	2	194	-186	64	207	34	72	0.5	12.4	0.92	0.8
11349	-11	2	19	-12	37	212	208	211	7.1	8.7	0.10	0.3
11952	24	2	-38	-86	-30	142	134	137	3.5	8.7	0.42	0.3
12306	-105	5	-146	-21	-30	249	199	202	5.1	12.9	0.44	0.3
13366	6	2	-46	-93	-74	154	127	147	3.3	8.8	0.45	0.8
14086	42	3	-17	-71	-14	151	149	159	4.2	8.6	0.34	0.1
14594	-140	2	-165	-110	-58	206	110	124	2.4	11.7	0.67	0.7
15394	8	2	-26	-45	-49	183	175	181	5.4	8.7	0.24	0.4
16214	151	4	84	-281	-92	138	-61	-110	1.2	9.7	0.77	1.5
17085	-5	3	-13	13	10	233	233	233	8.4	9.1	0.04	0.1
17147	120	2	100	-73	-38	182	147	152	3.8	9.9	0.45	0.3
17666	51	2	86	-100	-68	163	120	138	2.9	9.4	0.52	0.7
18235	98	1	17	-150	-18	74	70	72	1.4	8.6	0.72	0.1
18915	-26	2	30	-173	27	62	47	54	0.8	8.6	0.82	0.2
18995	-112	1	-80	-257	19	90	-37	-42	0.6	9.4	0.88	0.2
19007	37	3	43	23	7	246	243	243	7.9	10.5	0.14	0.1
19378	14	1	22	-51	49	178	169	176	5.3	8.8	0.25	0.6
19797	345	5	349	-130	-76	368	90	117	1.4	30.9	0.91	1.8
21000	45	3	34	6	-7	229	226	227	7.6	9.4	0.10	0.1
21586	41	3	67	-51	-3	182	169	169	4.8	9.3	0.32	0.0
21609	56	1	368	-126	35	381	94	100	1.5	34.7	0.92	0.7
21648	24	1	-228	-164	-176	293	56	184	0.9	83.6	0.98	68.9
21767	-3	3	-7	-4	16	216	216	216	7.7	8.6	0.06	0.1
22246	96	2	95	7	34	248	227	229	6.5	11.7	0.28	0.3
22632	111	6	54	-88	-23	144	132	134	3.4	8.9	0.44	0.2
23344	174	2	124	-155	-28	143	65	71	1.2	10.1	0.78	0.2
24316	232	1	198	-335	102	250	-115	-154	2.4	13.7	0.70	1.8
26688	2	3	-42	1	-35	228	221	224	7.3	9.5	0.13	0.3
27654	99	1	-26	-130	-35	100	90	97	2.0	8.6	0.62	0.3
28188	39	3	160	-32	-5	247	188	188	4.6	13.3	0.49	0.0
29759	242	2	264	-251	-28	268	-31	-41	0.4	17.0	0.95	0.3
29992	167	1	75	-154	18	101	66	68	1.3	9.1	0.75	0.1
30668	307	6	238	-175	-36	245	45	58	0.7	15.0	0.91	0.4
30990	60	2	77	-52	45	190	168	174	4.7	9.6	0.34	0.4
31188	47	7	17	-45	66	188	175	187	5.5	8.6	0.22	0.7
31639	53	3	-6	-39	-38	185	181	185	5.7	8.5	0.20	0.3
32308	105	3	78	-61	0	178	159	159	4.4	9.5	0.37	0.0
33582	-94	2	-212	-120	12	235	100	101	1.9	13.9	0.76	0.1
34146	-14	3	-39	5	2	229	225	225	7.5	9.6	0.12	0.0
34548	-28	3	-37	0	6	224	220	220	7.4	9.4	0.11	0.1
36491	91	2	49	-113	0	118	107	107	2.5	8.8	0.55	0.0
36849	-34	2	-67	-78	-46	163	142	149	3.8	9.2	0.42	0.4
37335	66	5	-170	-268	71	191	-48	-86	0.9	11.6	0.86	0.9
38541	-235	2	-270	-206	-82	282	14	83	0.2	17.4	0.98	1.4
38621	-108	8	20	-159	-124	139	61	138	1.3	9.5	0.76	2.4
38625	102	2	73	-53	8	183	167	167	4.7	9.4	0.34	0.1
40068	4	2	178	-352	244	330	-132	-278	5.1	18.0	0.56	10.5
40778	66	2	130	-246	32	136	-26	-41	0.4	10.1	0.92	0.3
42592	206	2	-253	-349	68	292	-129	-146	2.6	18.0	0.75	1.1
44075	121	1	40	-80	77	165	140	160	3.8	8.8	0.39	0.8
44116	17	3	-18	-2	36	222	218	221	7.7	8.8	0.07	0.3
44124	35	3	-191	-172	14	197	48	50	0.8	12.2	0.88	0.1
44716	170	2	119	-355	-75	195	-135	-154	3.3	10.7	0.53	1.1
44919	-36	9	-60	42	30	270	262	263	7.8	12.6	0.23	0.3
47139	110	8	18	-108	-2	113	112	112	2.8	8.7	0.51	0.2
47640	-14	3	-17	13	-5	234	233	233	8.3	9.2	0.05	0.1
48146	-2	3	-23	-4	2	218	216	216	7.5	8.9	0.09	0.1
48152	-15	3	-234	-225	-0	234	-5	-5	0.1	14.3	0.99	0.1
49371	-40	7	-134	-4	60	261	216	224	5.8	13.3	0.39	0.9
50139	-22	2	-80	-21	-15	215	199	199	5.8	10.1	0.27	0.1
50173	-36	1	-39	-117	20	112	103	105	2.6	9.2	0.56	0.7
52771	74	1	-163	-328	95	218	-108	-144	2.4	11.8	0.67	1.5
53070	65	2	26	-128	18	97	92	93	2.1	8.6	0.61	0.1
54858	-22	11	317	-303	-147	359	-83	-168	1.5	40.4	0.93	8.0
55022	62	2	-115	18	102	284	238	259	6.6	13.9	0.36	1.8
57265	198	2	367	-214	94	379	6	95	0.1	33.0	0.99	2.6
57850	229	4	2	-284	78	101	-64	-101	1.3	8.6	0.74	1.3
57939	-98	2	-284	-144	-7	295	76	77	1.2	19.2	0.88	0.1
58229	168	1	68	-194	57	92	26	63	0.4	8.9	0.91	0.6
58357	47	2	150	-163	44	167	57	72	1.0	10.8	0.83	0.5

TABLE 1. (continued)

HIP ^a	RV km/s	Ref ^b	U_{LSR} km/s	V_{LSR} km/s	W_{LSR} km/s	v_{RF} km/s	v_{ROT} km/s	h km/s	R_{min} kpc	R_{max} kpc	e	$ Z_{max} $ kpc
59109	58	2	94	-255	-85	132	-35	-92	0.6	9.3	0.89	1.1
59239	19	1	7	-101	76	141	119	141	3.1	8.7	0.47	1.0
59330	-37	3	-45	4	-18	229	224	225	7.4	9.7	0.13	0.2
59750	5	2	-61	-58	-53	181	162	170	4.6	9.1	0.33	0.5
60551	-3	2	85	-30	-9	208	190	190	5.5	10.0	0.30	0.1
60632	155	2	-117	-215	56	130	5	56	0.1	9.7	0.99	0.9
60719	6	1	128	-98	-14	178	122	123	2.8	10.4	0.57	0.3
61824	140	1	14	-109	120	164	111	164	3.0	8.9	0.50	2.6
62747	25	1	121	-510	-275	418	-290	-400	7.1	32.9	0.64	18.0
62882	152	9	-278	-194	-103	298	26	106	0.3	19.1	0.96	2.5
63970	-39	3	-29	8	-32	232	228	230	7.8	9.3	0.09	0.3
64115	74	5	180	-88	129	259	132	185	3.1	13.3	0.63	2.6
64426	49	2	73	-56	64	190	164	176	4.6	9.4	0.34	0.7
65268	-28	1	28	-10	-16	213	210	211	7.1	8.9	0.11	0.1
66246	-101	8	112	-65	-98	215	155	183	4.3	9.7	0.39	2.0
66509	-45	2	-71	-31	-54	209	189	197	5.6	9.6	0.26	0.5
66665	-25	2	-158	-85	-76	221	135	155	3.1	11.8	0.59	1.0
66815	-88	3	65	-6	-65	232	214	223	6.7	10.0	0.20	0.7
68594	-25	1	124	-205	22	126	15	27	0.2	9.7	0.96	0.3
68796	7	1	26	5	7	226	225	225	7.7	9.1	0.08	0.1
68807	155	7	-17	-193	111	116	27	115	0.4	8.5	0.90	1.6
69746	-121	8	290	-185	14	292	35	38	0.5	18.5	0.94	1.9
70647	149	1	-121	-227	-39	128	-7	-40	0.2	9.2	0.97	0.8
70681	-47	1	14	-34	-69	199	186	198	6.0	8.5	0.17	0.7
71886	-16	3	3	-1	-4	219	219	219	7.8	8.5	0.04	0.1
71887	-6	3	-2	30	-4	250	250	250	8.5	10.2	0.09	0.1
71939	-12	3	-4	34	-3	254	254	254	8.5	10.5	0.11	0.1
72461	33	2	-131	-94	26	184	126	129	2.9	10.5	0.57	0.3
73385	177	2	-51	-354	62	156	-134	-147	3.5	8.8	0.43	0.6
73960	-278	1	-6	-61	-282	324	159	324	8.0	11.5	0.18	8.6
74033	-61	2	105	-112	31	154	108	113	2.4	9.7	0.60	0.3
74067	-59	1	20	-53	-60	178	167	177	5.0	8.6	0.26	0.6
74079	19	3	-24	10	20	232	230	231	8.0	9.2	0.07	0.2
74234	312	2	-312	-495	-58	420	-275	-281	4.9	47.9	0.81	1.7
74235	311	2	-312	-495	-59	420	-275	-281	4.9	47.7	0.81	1.7
76976	-171	2	240	-239	48	246	-19	-52	0.2	14.7	0.97	0.6
77946	-65	1	131	-118	101	194	102	143	2.2	10.4	0.65	1.5
78640	-153	2	-117	-254	-18	123	-34	-38	0.5	9.7	0.90	0.2
80837	-48	2	-94	-251	-71	122	-31	-78	0.5	9.3	0.90	0.8
81170	-170	2	79	-159	-128	163	61	142	1.2	9.4	0.77	2.2
81461	-39	2	-3	-103	-12	118	117	118	2.9	8.4	0.49	0.1
85007	33	5	-47	26	10	251	246	247	7.9	10.8	0.16	0.1
85378	-73	2	56	-93	72	156	127	146	3.2	8.9	0.47	0.8
85757	4	2	-24	-69	72	169	151	167	4.3	8.5	0.33	0.7
85855	-285	2	104	-424	155	277	-204	-257	6.1	12.0	0.32	3.2
86013	-143	1	160	-53	83	246	167	186	4.0	12.7	0.52	1.2
86431	34	2	-212	-104	90	258	116	147	2.4	14.4	0.72	1.5
86443	-398	2	357	-238	84	368	-18	-86	0.3	29.9	0.98	2.1
87693	-243	2	-50	-372	-32	163	-152	-155	4.1	8.8	0.36	0.3
88010	186	2	-277	-272	39	284	-52	-65	0.8	17.8	0.92	0.5
88039	-16	1	-6	-100	83	146	120	146	3.1	8.5	0.46	0.9
91058	-36	5	57	17	-31	246	237	239	7.4	10.7	0.18	0.3
92167	-181	1	61	-68	-284	328	152	322	6.8	13.0	0.32	9.4
92532	-13	2	13	20	-35	243	240	242	8.4	9.5	0.06	0.3
92781	20	5	-111	-133	-25	143	87	90	1.8	9.6	0.69	0.2
94449	-66	2	-153	-301	60	183	-81	-101	1.5	10.8	0.75	0.7
96115	-124	1	-40	-143	-57	104	77	96	1.6	8.6	0.68	0.5
96185	-167	2	56	-150	63	110	70	94	1.4	8.8	0.72	0.6
97023	-9	5	-40	-16	-38	212	204	208	6.6	9.0	0.15	0.3
97468	-181	4	137	-196	-106	175	24	108	0.3	9.8	0.95	1.5
98020	-193	2	143	-102	69	198	118	136	2.6	10.9	0.61	0.8
98532	-15	1	-82	-115	51	142	105	116	2.4	9.2	0.58	0.5
99423	-115	3	21	-92	107	168	128	167	3.5	8.6	0.43	1.4
99938	-111	9	106	-64	-35	192	156	160	4.0	10.1	0.43	0.3
100568	-172	2	147	-231	-63	160	-11	-64	0.2	10.5	0.97	0.8
100792	-248	2	68	-264	-22	84	-44	-49	0.8	8.9	0.84	0.2
101346	-68	7	63	-26	3	204	194	195	5.8	9.4	0.24	0.0
101382	-6	2	20	10	48	236	230	235	8.1	9.2	0.06	0.4
103269	-131	2	-80	-131	-87	148	89	124	2.0	9.2	0.64	1.1
104659	-44	2	-100	-102	-51	163	118	129	2.8	9.6	0.55	0.5
104660	-102	1	119	-69	-30	194	151	154	3.7	10.5	0.48	0.3
105888	-85	2	26	-113	-36	116	107	113	2.5	8.5	0.54	0.3
106947	-104	5	55	-59	75	186	161	177	4.6	9.0	0.33	0.8
107975	19	1	-22	28	-0	249	248	248	8.3	10.2	0.10	0.0
109067	-201	2	27	-208	39	48	12	40	0.2	8.6	0.96	0.3
109390	-16	2	-122	-121	17	158	99	100	2.2	9.8	0.64	0.4
109558	-291	2	293	-265	12	296	-45	-47	0.7	19.4	0.93	0.2
112796	-116	4	-277	-234	82	289	-14	-83	0.1	18.0	0.99	1.6
114271	-32	10	-12	-92	1	128	128	128	3.3	8.5	0.44	0.1
114962	16	2	-392	-317	-53	407	-97	-111	1.4	43.2	0.94	1.5
115167	-246	5	291	-439	-55	369	-219	-226	4.3	30.1	0.75	1.3
115610	-42	3	-123	-44	-65	224	176	188	4.6	11.2	0.41	0.8

TABLE 1. (continued)

HIP ^a	RV km/s	Ref ^b	U_{LSR} km/s	V_{LSR} km/s	W_{LSR} km/s	v_{RF} km/s	v_{ROT} km/s	h km/s	R_{min} kpc	R_{max} kpc	e	$ Z_{max} $ kpc
115949	-119	1	-152	-133	-59	185	87	105	2.1	11.0	0.69	0.9
116082	27	3	34	20	-22	244	240	241	8.0	10.2	0.12	0.2
117029	-71	1	62	-92	89	168	128	156	3.3	9.1	0.46	1.1
117041	-86	2	239	-166	-190	310	54	198	1.2	52.0	0.95	39.3
G97-40	2	2	-140	-588	85	403	-368	-378	8.2	40.4	0.7	2.8
G110-43	26	2	-64	-227	-160	172	-7	-160	0.1	13.2	1.0	4.6
G88-42	390	2	138	-643	144	468	-423	-447	8.4	76.3	0.8	8.9
G90-36	268	2	206	-511	-40	359	-291	-294	6.1	29.8	0.7	0.8
G114-42	-87	2	-358	-165	-70	369	55	89	0.6	31.8	1.0	1.7
G116-53	114	2	-337	-91	107	376	129	168	3.4	42.6	0.9	5.4
G197-30	137	2	413	-163	44	419	57	72	0.7	49.5	1.0	1.2
G166-37	369	2	-295	-126	341	461	94	354	2.2	53.6	0.9	39.5
G15-13	219	2	-223	-428	163	346	-208	-264	4.8	22.0	0.6	5.3
G16-25	23	2	-73	-557	160	380	-337	-373	8.0	26.9	0.5	5.7
G93-1	-121	2	-332	-462	-91	421	-242	-259	3.8	46.9	0.8	4.4

^aThe first 9 columns of data for the Stephens 1999 stars (those with Giclas numbers) are taken directly from the Carney *et al.* 1994 survey. The orbital parameters (R_{min} , R_{max} , e , and $|Z_{max}|$) were recalculated using the same galactic potential as the F00 stars.

^bReferences: (1) HIC, (2) CLLA, (3) F00 spectra, (4) Bond 1980, (5) Sandage & Fouts 1987, (6) Beers *et al.* 2000, (7) Norris 1986, (8) Chiba & Yoshii 1998, (9) Beers & Sommer-Larson 1995, (10) Stetson 1983 and (11) Bartkevicus *et al.* 1992.

TABLE 2. Abundance Ratios as a Function of Rest-Frame Velocity for $-1 > [\text{Fe}/\text{H}] > -2$

Quantity	$v_{RF} < 150$			$150 < v_{RF} < 300$			$v_{RF} > 300$		
	Mean	sdom	n	Mean	sdom	n	Mean	sdom	n
T_{eff} (K)	5354	138	21	5218	85	31	5300	98	21
$\log(g)$	3.1	0.3	21	3.2	0.2	31	4.0	0.2	21
[Fe/H]	-1.61	0.05	21	-1.49	0.06	31	-1.52	0.05	21
$\log n(\text{Li})$	+2.07	0.13	12	+1.55	0.16	17	+1.48	0.28	17
[Na/Fe]	-0.07	0.03	21	-0.10	0.03	30	-0.34	0.05	21
[Mg/Fe]	+0.44	0.02	21	+0.41	0.02	31	+0.22	0.03	21
[Al/Fe]	+0.24	0.05	7	+0.24	0.04	14	-0.02	0.13	5
[Si/Fe]	+0.47	0.02	20	+0.40	0.02	30	+0.31	0.03	17
[Ca/Fe]	+0.34	0.02	21	+0.32	0.01	31	+0.24	0.02	21
[Ti/Fe]	+0.31	0.02	20	+0.29	0.02	31	+0.26	0.03	21
[V/Fe]	-0.01	0.05	7	+0.00	0.02	27	-0.02	0.10	8
[Cr/Fe]	-0.08	0.02	20	-0.04	0.01	30	-0.02	0.01	21
[Ni/Fe]	+0.01	0.01	21	+0.00	0.01	30	-0.06	0.02	21
[Y/Fe]	-0.02	0.04	16	-0.05	0.04	24	-0.17	0.04	19
[Zr/Fe]	+0.25	0.08	13	+0.26	0.05	21	+0.19	0.05	6
[Ba/Fe]	+0.08	0.04	21	+0.07	0.03	30	-0.02	0.03	21
[Eu/Fe]	+0.36	0.05	7	+0.41	0.05	15	+0.44	0.06	6
[Y/Zr]	-0.29	0.06	13	-0.32	0.03	21	-0.35	0.10	6
[Ba/Eu]	-0.21	0.11	7	-0.40	0.06	15	-0.49	0.07	6
v_{RF} (km s^{-1})	120	5	21	212	9	31	389	8	21
v_{ROT} (km s^{-1})	47	18	21	39	20	31	-108	43	21
h (km s^{-1})	43	20	21	42	24	31	-88	57	21
R_{max} (kpc)	9.1	0.1	21	14.3	2.4	31	37.4	3.1	21
$ Z_{max} $ (kpc)	0.6	0.1	21	3.1	2.2	31	6.2	1.9	21
e	0.72	0.04	21	0.66	0.05	31	0.76	0.05	21